

Formation of a high-density skyrmion crystal in the monolayer semiconductor LiCrTe_2 with tunable bands

Mingliang Liu ^{1,2}, Jia-Tao Sun ^{3,*} and Sheng Meng ^{1,2,4,†}

¹*Beijing National Laboratory for Condensed Matter Physics and Institute of Physics, Chinese Academy of Sciences, Beijing 100190, China*

²*School of Physical Sciences, University of Chinese Academy of Sciences, Beijing 100049, China*

³*School of Integrated Circuits and Electronics, MIIT Key Laboratory for Low-Dimensional Quantum Structure and Devices, Beijing Institute of Technology, Beijing 100081, China*

⁴*Songshan Lake Materials Laboratory, Dongguan, Guangdong 523808, China*



(Received 13 September 2024; revised 15 December 2024; accepted 28 January 2025; published 18 February 2025)

Skyrmions, as unique wrapped spin textures, hold great potential for next-generation spintronic devices. Here, we reveal the emergence of nontrivial spin textures in the monolayer semiconductor LiCrTe_2 through a combination of first-principles calculations and micromagnetic simulations, which evolve into a Néel-type skyrmion crystal (SkX) in response to external magnetic fields at finite temperatures. The monolayer can sustain a high density of skyrmions, reaching up to 0.018 skyrmions/ nm^2 with a diameter of 2.9 nm, which surpasses values in previous reports for semiconductor layers. The synergistic effect of temperature and magnetic field on the formation of a SkX has been identified. Furthermore, we observe an inverse relationship between the electronic band gap and the skyrmion size in the SkX. Notably, the band gap closes and reverses as the size of skyrmions increases when the monolayer is compressed by -3% in-plane biaxial strain, highlighting the tunable interplay between real-space and reciprocal-space spin textures. Our results shed light on the evolution of a SkX in a semiconducting monolayer and demonstrate the transition of topological and electronic properties upon the generation of a SkX, providing valuable insights for experimental realization and future spintronic applications.

DOI: [10.1103/PhysRevB.111.054423](https://doi.org/10.1103/PhysRevB.111.054423)

I. INTRODUCTION

Skyrmions are magnetic configurations characterized by swirling topological spin textures. They are anticipated to play a crucial role not only in fundamental physics, such as the topological Hall effect, but also in innovative device applications, including quantum computing and advanced instrumentation [1–7]. Skyrmions possess a topologically nontrivial spin quasiparticle, which has high efficiency in information transfer and storage [8,9]. Consequently, one of the primary areas of interest in magnetic materials research is magnetic skyrmions. Authors of previous studies have found magnetic skyrmions in many alloy or metal compounds [10–12], and current investigators are concentrating on magnetic skyrmions in layered two-dimensional (2D) materials, particularly those that are compatible with semiconductor technology. Researchers have discovered noncollinear spin textures in various monolayers as well as in bilayer heterostructures [13–16]. Authors of other theoretical studies have predicted that the formation of skyrmions depends on the parameters of magnetic interactions [17,18]. Transport properties have been identified in 2D skyrmions materials, including the topological Hall and topological Kerr effects [19,20]. Complex spin textures periodically arranged in real space can behave as quasiparticles, significantly influencing the topological

Hall effect and the magnon bands in a skyrmion crystal (SkX) [21,22]. These properties are strongly correlated with the density and distribution of skyrmions, prompting further research into SkXs with higher density and improved controllability.

Intrinsic and alkali-decorated chromium chalcogenide monolayer compounds exhibit numerous appealing magnetic properties. The intrinsic CrTe_2 layer can perform a noncollinear antiferromagnetic (AFM) state [23], and calculations indicate that it possesses a high Curie temperature >200 K when alkali atoms are attached to the layer [24]. Inspired by spin textures and skyrmions observed in similar materials such as CrSSe and CrInSe_3 [25,26], authors of theoretical studies have also identified spin textures and potential skyrmion states in LiCrTe_2 [27]. In an experiment, sodium-attached CrSe_2 bulk was prepared and exfoliated into single layers [28], and bulk LiCrTe_2 was confirmed to maintain an AFM state at 125 K with magnetic anisotropy and Dzyaloshinskii-Moriya interaction (DMI) effects [29,30]. Notably, the skyrmion-induced topological Hall effect was detected in $\text{Cr}_{0.87}\text{Te}$ [31], and Néel-type skyrmions were observed in self-intercalated $\text{Cr}_{1+\delta}\text{Te}_2$ above room temperature [32]. Although authors of previous studies gave remarkable magnetic properties of the chromium chalcogenide system, the periodic arrays of skyrmions in 2D alkali-decorated CrTe_2 remain to be fully investigated. Furthermore, researchers have found electronic bands controlled by collinear spin direction in 2D magnets [33], but materials with electronic bands tuned by spin textures in a SkX still necessitate further exploration.

*Contact author: jtsun@bit.edu.cn

†Contact author: smeng@iphy.ac.cn

In this paper, we delve into the periodic formation of skyrmions in single-layer LiCrTe₂, scrutinizing the effects of temperature and magnetic fields and the electronic band structures of a SkX through density functional theory (DFT) calculations along with micromagnetic simulations. The magnetic properties of LiCrTe₂ demonstrate the formation of a high-density SkX. During the evolution of spin textures, the external magnetic field optimizes the distribution of skyrmions, while temperature facilitates the dissolution of metastable states. This contributes to the emergence of high-density skyrmions and the generation of a SkX. Our calculations further reveal that with the enlargement of skyrmions, the band gap of a SkX decreases, transforming from an indirect to a direct band gap. Additionally, we have observed band crossing and a reversal of spin chirality in reciprocal space when the size of skyrmion decreases under compressive strain, indicating the intricate interplay of complex spin textures between real and reciprocal spaces. Our findings enhance the understanding of skyrmion generation in LiCrTe₂ and has implications for exploring the potential of a SkX in 2D semiconducting magnetic materials for spintronic applications.

II. METHODS

A. First-principles calculations

We performed first-principles calculations using VASP [34], employing the Perdew-Burke-Ernzerhof exchange-correlation functional and the projector augmented-wave method in DFT calculations [35,36]. The phonon dispersion was determined using density functional perturbation theory with PHONOPY [37]. A plane-wave cutoff energy of 500 eV was applied, and a Coulomb Hubbard term U of 3 eV was set on the d orbital of the Cr element. The atomic structure of LiCrTe₂ was optimized until the force on each atom was $<10^{-3}$ eV/Å, with an electronic iteration convergence threshold of 10^{-8} eV for a unit cell and 10^{-6} eV for a supercell. To avoid spurious interactions from periodic images, a 16 Å vacuum layer was included. Spin-orbit coupling was included in all DFT calculations. Self-consistent calculations utilized an $8 \times 8 \times 1$ Γ -centered k -mesh in momentum space, and the Γ point for larger supercells. Supercell calculations of a SkX were conducted with fixed atomic structures, allowing relaxation only for magnetic moments and electronic structures. The DFT calculations for skyrmions specified the magnetic moments in the supercell as Néel- or Bloch-type skyrmions to ensure the SkX under periodic boundary conditions in the in-plane directions. The magnetic moments of Cr atoms were not constrained and were allowed to be optimized during the self-consistent relaxation.

B. Micromagnetic simulations

The real-space complex spin textures were calculated by micromagnetic simulation using the MUMAX3 package with the Landau-Lifshitz equation [38]. We set a 128×128 supercell with a unit size of 4.12×7.15 Å to simulate the rectangular unit cell of monolayer LiCrTe₂. The thickness of the layer is set as 4.30 Å, which matched the effective thickness of the optimized LiCrTe₂ monolayer. The time step in each

simulation was set as 10^{-5} ns. Periodic boundary conditions were enforced. Landau-Lifshitz damping constant α was set to 0.2 with the Dormand-Prince method of the Runge-Kutta solver used to advance the solution of the Landau-Lifshitz equation, which contained a fourth-order error estimate and fifth-order convergence. The external magnetic field was set in the $+z$ direction, consistent with the uniaxial magnetic anisotropy direction. Random magnetic (RM) states were initialized with random spin directions in each unit cell originally.

III. RESULTS AND DISCUSSION

A. Structural and magnetic parameters

The fully relaxed atomic structure of Li-decorated 1T-CrTe₂ is depicted in Fig. 1(a). The obtained lattice constant for monolayer LiCrTe₂ is 4.12 Å, which is consistent with previous findings [24,27]. The top lithium adsorption in LiCrTe₂ disrupts the symmetry of 1T-CrTe₂ and introduces DMI into the monolayer. The estimated phonon band dispersion shows no imaginary frequency mode, indicating that this monolayer structure is dynamically stable (refer to Fig. S1 in the Supplemental Material [39]). We described the magnetic Hamiltonian model of this 2D system as follows:

$$H = - \sum_{i,j} J_{ij} \mathbf{S}_i \cdot \mathbf{S}_j - \sum_{i,j} \mathbf{D}_{ij} \cdot (\mathbf{S}_i \times \mathbf{S}_j) - \sum_i K_u (\mathbf{S}_i^z)^2 - \sum_i \mu_m \mathbf{B} \cdot \mathbf{S}_i + E_{\text{other}}, \quad (1)$$

where \mathbf{S} denotes the spin vectors. Here, J , \mathbf{D} , K_u , and μ_m represent the Heisenberg interaction, DMI, single-ion anisotropy, and magnetic moment of chromium atoms, respectively. Also, \mathbf{B} represents the external magnetic field, and other energies such as dipole interaction are not considered. To determine the magnetic parameters responsible for the magnetization energy in the Hamiltonian model of LiCrTe₂, we employed the four-state method to calculate the DMI and Heisenberg exchange coefficients [40,41]. The energies of various spin configurations were computed using a 5×4 supercell. By altering the spin directions of two adjacent Cr atoms within a vertical plane including both atoms (while the spins of other Cr atoms in the supercell remained parallel and out-of-plane), we obtained the in-plane component of DMI to be 4.81 meV per unit cell for the nearest-neighbor Cr atoms. The DMI direction is perpendicular to the line connecting the two Cr atoms. The out-of-plane component of DMI was calculated by adjusting spins in the monolayer plane and was found to be nearly zero due to the symmetry of the in-plane spins. The Heisenberg interaction between the first, second, and third nearest neighbors were calculated to be $J_1 = 24.91$ meV, $J_2 = 0.63$ meV, and $J_3 = -1.73$ meV per unit cell, respectively. Our results align with the values reported in previous calculations [27,42]. For further details on the four-state method, please refer to the Supplemental Material [39].

With the different neighboring Heisenberg interaction energies of LiCrTe₂, we further calculated the magnetic exchange stiffness, denoted as $A = \frac{1}{2V} \sum_i J_i(r_i)^2$, with a value of 6.42×10^{-12} J/m. The r_i represents the distances between various magnetic Cr atoms, considering the first, second,

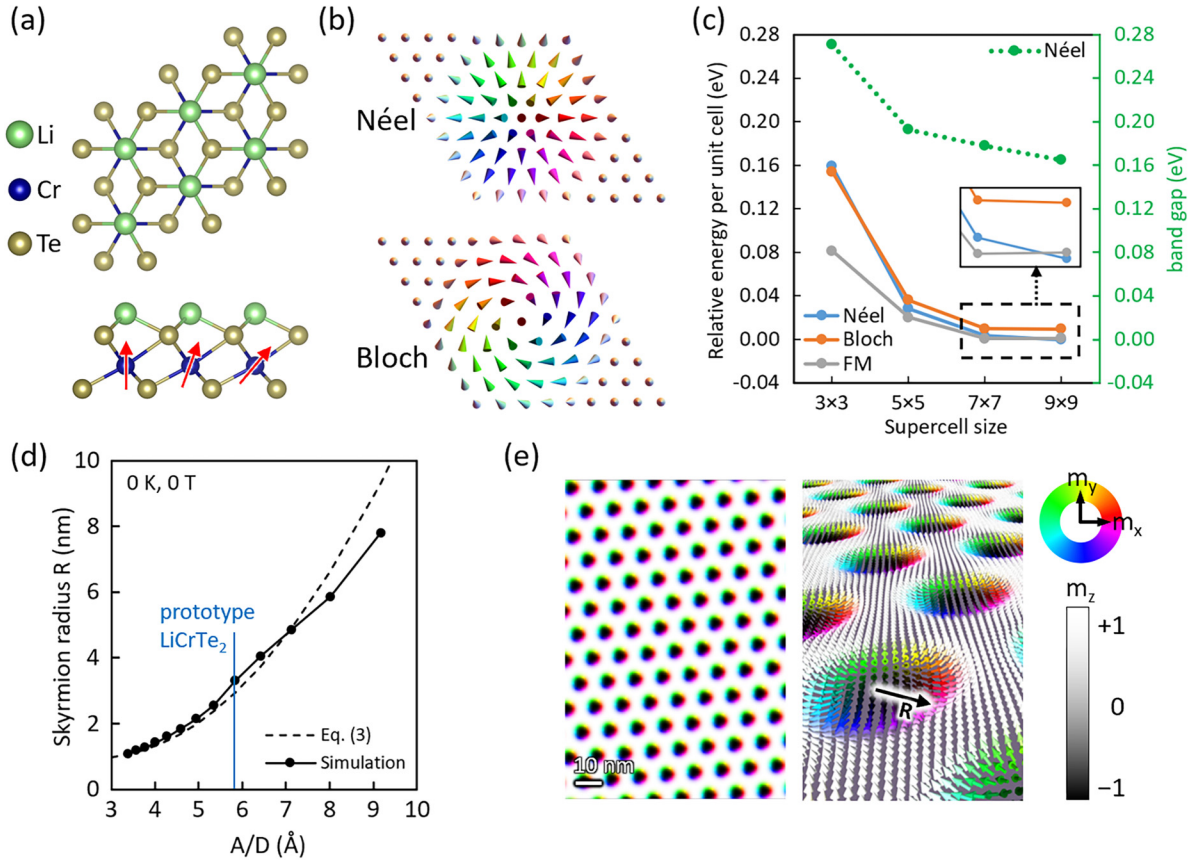


FIG. 1. Atomic and magnetic structure of LiCrTe_2 . (a) Atomic structure of single-layer LiCrTe_2 . The Cr atoms are off-center from the normal 17-CrTe_2 structure. The red arrows show the noncollinear spins. (b) The adopted magnetic configuration of Néel- and Bloch-type skyrmion crystal (SkX). Each arrow represents one spin of Cr atom in the LiCrTe_2 supercell. (c) The calculated relative energy per unit cell of LiCrTe_2 supercells considering Néel (blue) and Bloch (orange) skyrmions and ferromagnetic magnetization (gray). The green dashed line is the calculated band gap of Néel-type SkX. (d) The dependence of skyrmion radius R (black dots) in SkX on the ratio of exchange stiffness A and in-plane Dzyaloshinskii-Moriya interaction (DMI) D without magnetic field. The dashed line represents the radius calculated by the model function presented in Eq. (2). (e) SkX in LiCrTe_2 obtained by micromagnetic simulation under magnetic field of 5 T at zero temperature. The left panel shows the top view, and the right panel shows the perspective magnetic configuration of Néel-type SkX.

and third nearest neighbors, each associated with their corresponding J_i . This signifies the strength of parallel interactions among neighboring spins. The in-plane DMI parameter was calculated using the formula $D = \frac{1}{V} \sum_i D_i r_i$, resulting in a value of 0.01128 J/m^2 . Here, D_i refers to the DMI energies arising from neighboring spins, which contribute to the formation of noncollinear spin textures. We considered the in-plane DMI of the nearest-neighbor Cr atoms. Other magnetic parameters such as saturation magnetization $M_s = 6.83 \times 10^5 \text{ A/m}$ and magnetic anisotropy $K_{u1} = 1.59 \times 10^6 \text{ J/m}^3$ can be directly obtained from DFT calculations. The magnetic crystalline anisotropy energy was determined to be 0.42 meV per unit cell by analyzing the total energy difference between the magnetic moments in the in-plane and perpendicular out-of-plane directions. These parameters can be used to evaluate the threshold parameter of the SkX, which is scrutinized by $\kappa = \frac{\pi^2 D^2}{16AK}$. If κ is significantly > 1 , the magnetic system tends to form a SkX since the strength of DMI plays a more prominent role than Heisenberg interaction and magnetic anisotropy [43]. The calculated $\kappa = 7.71$ indicates the occurrence of a SkX in LiCrTe_2 .

To verify the stability of the SkX in LiCrTe_2 , we conducted DFT calculations using supercells of LiCrTe_2 considering various magnetic configurations, including ferromagnetic (FM), spin-wrapped Néel-type, and Bloch-type skyrmions. Figure 1(b) schematically depicts the spin textures of the two types of skyrmions. Each supercell contains one skyrmion with periodic boundary conditions adopted in DFT calculations. The initial magnetic configurations of Cr sites in the supercell of DFT calculations were established by the following function:

$$\mathbf{m}(\mathbf{r}_i) = (m_x, m_y, m_z) = m_0 \left[\cos \left(\frac{\pi}{2} - \frac{|\mathbf{r}_i|}{R} \pi \right) \cdot \frac{r_x}{|\mathbf{r}_i|}, \right. \\
 \left. \cos \left(\frac{\pi}{2} - \frac{|\mathbf{r}_i|}{R} \pi \right) \cdot \frac{r_y}{|\mathbf{r}_i|}, \sin \left(\frac{\pi}{2} - \frac{|\mathbf{r}_i|}{R} \pi \right) \right], \quad (2)$$

where $m_0 = 3.5\mu_B$ represents the magnitude of magnetic moment of Cr atom, and R denotes the radius of the skyrmion that multiplies the lattice constant by half of the supercell size. The vector \mathbf{r}_i represents the positions of other Cr atoms relative to the central atom, with r_x and r_y indicating the coordinates. The

magnetic moment of the central Cr atom was oriented perpendicular to the layer, as we utilized a supercell composed of an odd number of unit cells. The spins of Cr atoms located at a distance exceeding R from the center were aligned normal to the plane and opposite that of the central Cr atom. The calculated relative energy per unit cell is shown in Fig. 1(c), which clearly shows that the energy of a Néel-type skyrmion is lower than that of the Bloch type. Furthermore, the total energy of a SkX per unit cell within the 9×9 supercell is lower than that of the FM state, as shown in the inset of Fig. 1(c). During the self-consistent calculation, the magnetic moments were unconstrained, enabling the optimization of both size and orientation. The relaxed spins preserved a skyrmion texture within the supercell. These first-principles results underscore the enhanced stability of noncollinear Néel-type skyrmions in LiCrTe₂. The electronic band gap of the supercell in Fig. 1(c) indicates that this skyrmion lattice is a semiconductor, providing potential to be controlled by external fields in experiments and electronic devices. More details about the band structures of SkX will be discussed later in Sec. III D.

Since the emergence of Néel-type skyrmions is verified, we conducted micromagnetic simulations using the previously determined magnetic parameters. Micromagnetic simulation serves as a numerical approach for solving magnetic dynamics, playing a crucial role in analyzing the stability of various spin textures. The presence of in-plane DMI fosters the formation of Néel-type skyrmions in micromagnetic simulation, consistent with the DFT results presented in Fig. 1(c). We first evaluated the size of skyrmions with a theoretical model. The skyrmion radius R is a fundamental quantity of a SkX which can be described by the following model [17,18]:

$$R = \frac{0.54}{\sqrt{n}} - \frac{A}{D} \sqrt{\frac{0.51}{\sqrt{n} \frac{A}{D} + 0.56n \frac{A^2}{D^2} - 0.02 \frac{16AK}{\pi^2 D^2}}}, \quad (3)$$

where Eq. (3) depends sensitively on magnetic exchange stiffness A , magnetic anisotropy energy K , DMI D , and skyrmion density n . Here, R represents the skyrmion radius where the spin direction transitions from out-of-plane to in-plane from the center. The skyrmions density n of specific A/D can be obtained from simulation results that started with random initial magnetic spin textures. The computed skyrmion radius as a function of the magnetic parameter ratio of A/D is shown in Fig. 1(d), where the radius from model predictions of Eq. (3) (dashed line) and the results from micromagnetic simulations (black dots) agree well with each other. The skyrmion radius decreases with an increase in D or a decrease in A in the absence of an external magnetic field. The skyrmion radius for the SkX in the LiCrTe₂ monolayer is 2.9 nm calculated by this model, consistent with 3.3 nm from micromagnetic simulation and equivalent to 7 unit cells in DFT calculation. Subsequently, we applied an external field to obtain an ideal SkX lattice in micromagnetic simulations. As shown in Fig. 1(e), our simulations successfully revealed the perfect lattice of a Néel-type SkX in monolayer LiCrTe₂, which originates from RM states under a 5 T external magnetic field at extremely low temperature (<10 K in practice). Since the SkX under investigation is subjected to external magnetic fields, the size of skyrmions can be reduced to a radius of 3–6 unit cells.

B. Evolution of topological skyrmions

After establishing the emergence of a SkX, we analyze the formation of a SkX in single-layer LiCrTe₂. The evolution of a SkX is characterized by the topological charge of spin textures, which is typically quantified by the winding number as [13]

$$Q = \frac{1}{4\pi} \int \mathbf{m}(r) \cdot [\partial_x \mathbf{m}(r) \times \partial_y \mathbf{m}(r)] d^2r, \quad (4)$$

where $\mathbf{m}(r)$ refers to each localized magnetic moment. The topological charge Q is approximately equal to the number of skyrmions in a SkX, and the topological Hall effect is also characterized by Q , where a higher Q leads to larger topological Hall conductivity. Figure 2(a) shows the obtained topological charge of the LiCrTe₂ layer as a function of external magnetic field at zero temperature. Each simulation ran for 1 ns from a RM to imitate the evolution of disordered noncollinear spins. The topological charge density rises as the ramified magnetic stripes evolve to skyrmions with increasing magnetic field strength, reaching a maximum of 0.018 nm^{-2} at 8 T external field in the SkX. The system transitions to fully parallel-aligned spins at magnetic fields >13 T, causing the topological charge density to decrease to zero.

To investigate the influence of finite temperatures on the formation of skyrmions, we conducted simulations from FM initial states. If the simulation commenced from a FM initial state at a very low temperature, the spin textures would remain in FM states until the temperature is increased sufficiently to disrupt the parallel spins (see Fig. S3 in the Supplemental Material [39]). The energy of spin textures featuring stripes and skyrmions was lower than that of the FM state, indicating that the layer exhibited a metastable FM state at very low temperatures. Thus, we conducted simulations starting from FM states at a higher temperature of 120 K. Figure 2(b) shows the final topological charge density of spin textures under different magnetic fields, indicating that skyrmions emerged from the FM region when the temperature cooperated with magnetic fields. The topological charge density reaches a maximum of $9.4 \times 10^{-2} \text{ nm}^{-2}$ under an external field of 6 T and decreases to zero under 12 T. Consequently, we infer that finite temperature can induce thermal fluctuations in the LiCrTe₂ layer, disrupting the FM state and facilitating the formation of skyrmions within the FM region.

Figure 2(c) illustrates the evolution of topological charge density in two specific simulations. The orange line corresponds to the orange point in Fig. 2(a), which evolved to a SkX under a magnetic field of 5 T at extremely low temperature. The spin textures at various time stamps are visualized in Fig. 2(d). During evolution, the scattered spins rapidly coalesced into magnetic domains, which then gradually shrank into skyrmions under the influence of the magnetic field. Once all the spin textures became skyrmions of ~ 3 nm in radius, they started to optimize the separation and eventually formed a SkX with a triangular lattice. Since the skyrmions are topologically protected spin textures, the total topological charge remained constant throughout the evolution after 0.01 ns. Another evolution was simulated under a magnetic field of 5 T at 120 K from the FM state. Details of the spin textures are shown in Fig. 2(e). In this case, random

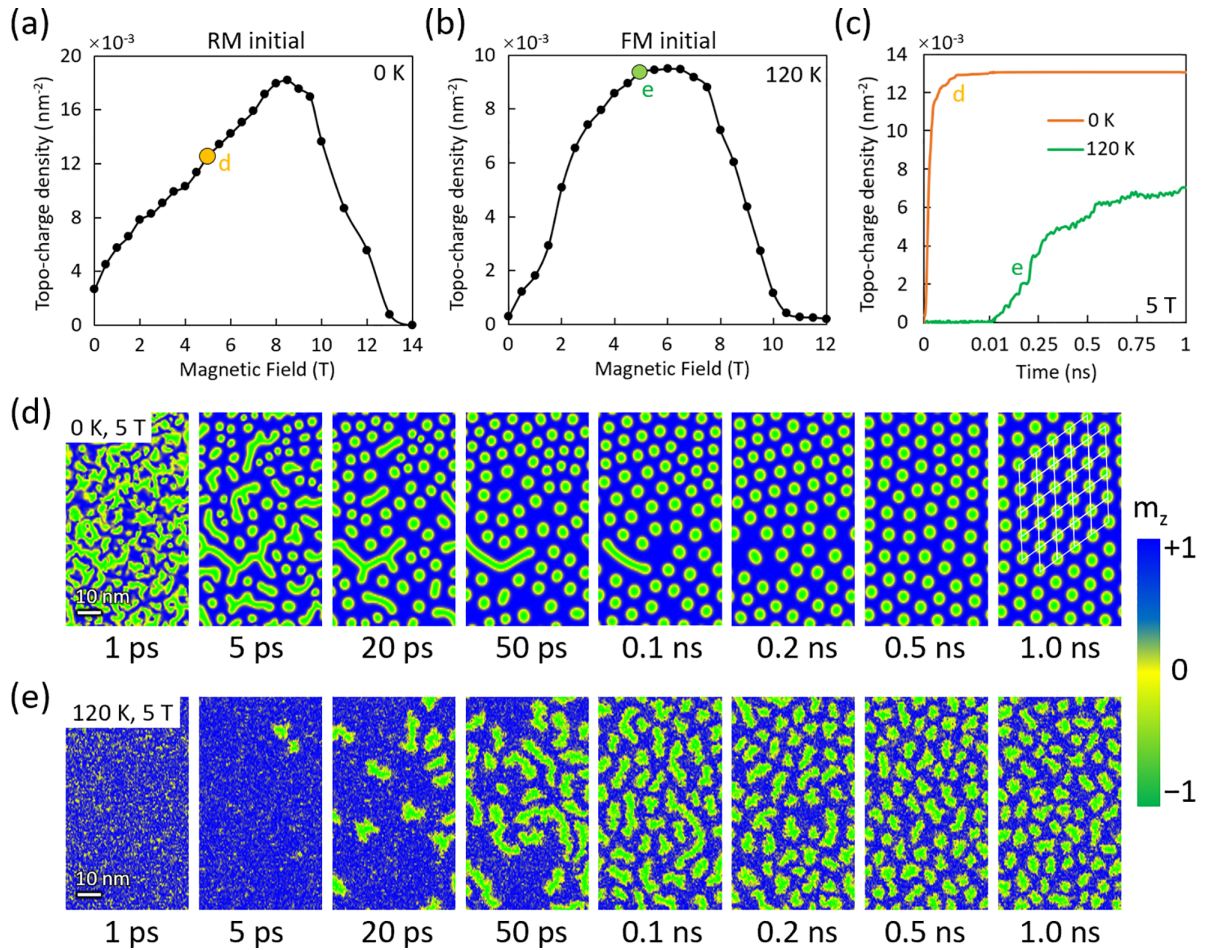


FIG. 2. The evolution of topological charge density of skyrmions in LiCrTe_2 . (a) The topological charge density of spin textures in LiCrTe_2 layer as a function of magnetic fields. The micromagnetic simulations started from random magnetic (RM) states under 0 K. (b) The topological charge density of spin textures simulated from ferromagnetic (FM) states under 120 K. (c) The topological charge varies over time during the relaxation process of two specific simulations. (d) Spin textures at specific times from the orange line in (c), with eight panels show the evolution of a skyrmion crystal (SkX) that developed from a RM state under a magnetic field. The SkX converged at 1 ns contains 66 skyrmions. (e) Spin textures from the evolution process corresponding to the green line in (c), where the skyrmion lattice emerges from a FM state under a 5 T magnetic field.

thermal fluctuations caused skyrmions and magnetic domains to gradually emerge in the FM region because the magnetization energy favored the formation of spin textures. The magnetic field further sliced the developing magnetic domains into individual skyrmions, resulting in a dynamic equilibrium with fluctuating skyrmions in the SkX. As demonstrated above, temperature and magnetic field have a significant impact on the production and temporal evolution of a SkX. Finite temperature introduces perturbations to the spin textures, disrupting the metastable FM region. Meanwhile, the magnetic field reshapes the stripe domains, transforming them into skyrmions. These changes lead to an increase in topological charge and enhance the periodic array of skyrmions, resulting in formation of a SkX.

C. Phase diagram of complex spin textures

To further investigate the phase diagram of spin textures, we performed micromagnetic simulations of the LiCrTe_2

monolayer across a broader range of temperatures and external magnetic fields. The topological charge density Q of various spin textures evolving from RM states for 1 ns under different conditions is depicted in Fig. 3(a). Simultaneously, Fig. 3(b) illustrates the distribution of average magnetization M per unit cell. Several states are delineated in the phase diagram. The spin textures form stripes and skyrmions under magnetic field < 4 T at lower temperatures, while a SkX becomes prominent in the range of 4–9 T. However, magnetic fields > 10 T tend to disrupt the skyrmion structures by aligning the spins parallel to the field direction, leading to very low topological charge and eventually transition to the FM state. At temperatures > 200 K, the boundaries of skyrmions are disrupted, leading to a disordered magnetization state characterized by chaotic spin textures.

As stated above, the SkX can be obtained within a temperature range of 0–150 K and a magnetic field range of 4–9 T. The highest density of the SkX, marked at 0.018 nm^{-2} , is notably found at temperatures < 30 K under external field of 8 T, high-

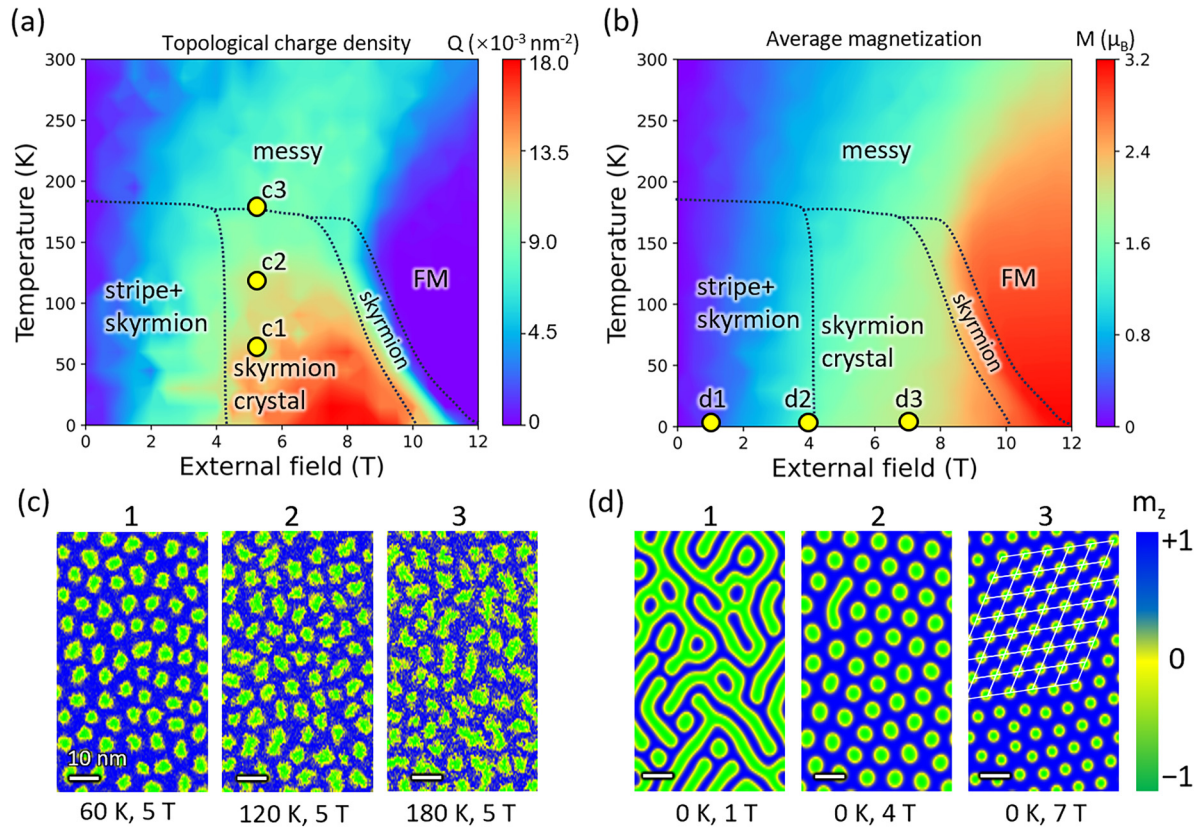


FIG. 3. Phase diagram of spin textures in LiCrTe_2 as a function of the temperature and external magnetic field. (a) Topological charge density of LiCrTe_2 layer after relaxing for 1 ns starting from random magnetic states. The color bar indicates the density of topological charge Q . Different types of spin textures are divided into several regions. (b) Average magnetization per unit cell along $\pm z$ direction from the same simulation conditions. The unit cell here refers to primitive atomic lattice of LiCrTe_2 , with each unit cell containing one Cr atom. μ_B is Bohr magneton. The color bar indicates the magnetization M . (c) and (d) Evolved spin textures refer to yellow dots in the phase diagrams. All skyrmions and stripes in these simulations are Néel type. As the phase of spin textures changes gradually with temperature or field, the boundary between different states is smooth with mixed components.

lighting the optimal conditions for SkX formation in terms of temperature and magnetic field strength. Figure 3(c) illustrates the evolution of a SkX when the temperature increases under a 5 T magnetic field, where the perfect lattice of the SkX is gradually disrupted by higher temperatures. Figure 3(d) shows spin textures under increasing external magnetic fields at a constant temperature. In this scenario, the magnetic domains are truncated or reduced in size by the applied field, gradually transforming into skyrmions. This observation suggests that a moderate magnetic field promotes the emergence of a SkX and enhances the density of topological charge. The magnetic field significantly affects the size of skyrmions, reducing their diameters in the SkX to 4.8, 4.2, and 2.9 nm under magnetic fields of 5, 7, and 10 T at zero temperature, respectively. The highest obtained density of skyrmions in LiCrTe_2 is higher than that of other 2D semiconductor materials in previous reports, such as 0.012 nm^{-2} in CrSSe , 0.015 nm^{-2} in CrInTe_3 , and 0.011 nm^{-2} in heterobilayer $\text{CrI}_3 - \text{CrCl}_3$, and competitive with skyrmion size in 2D metals [25,26,44,45]. Based on the phase diagram results, the random initial magnetization undergoes reorganization in response to the external field. The topological charge of the SkX increases as the size of skyrmions decreases under higher field until it transitions to a FM state, while lower temperature guarantees a more

stable topological charge during optimization process of spin textures.

D. Electronic band structures in Néel-type SkX

Authors of previous studies on skyrmion lattices have primarily focused on magnon bands. However, the interaction between a real-space SkX and reciprocal electronic band structures remains an area ripe for exploration. To delve into this point, we conducted first-principles calculations to examine the band structure of a SkX in monolayer LiCrTe_2 . The electronic band gaps of a SkX with different sizes of skyrmions are shown in Fig. 1(c). In comparison with the indirect band gap of 0.139 eV for the FM LiCrTe_2 unit cell, the band gap of skyrmions in a 3×3 supercell increases to 0.271 eV due to excessive spin wrapping [39]. When the skyrmion size increases to 5×5 and 7×7 supercells as spin textures shown in the upper and lower panel in Fig. 4(a), the band gap decreases to 0.193 eV and further to 0.178 eV, respectively, as shown in Figs. 4(b) and 4(c). Moreover, the indirect band gap becomes direct in a 7×7 supercell. These underscore the intricate relationship between spatial SkX density and reciprocal band structures, presenting an

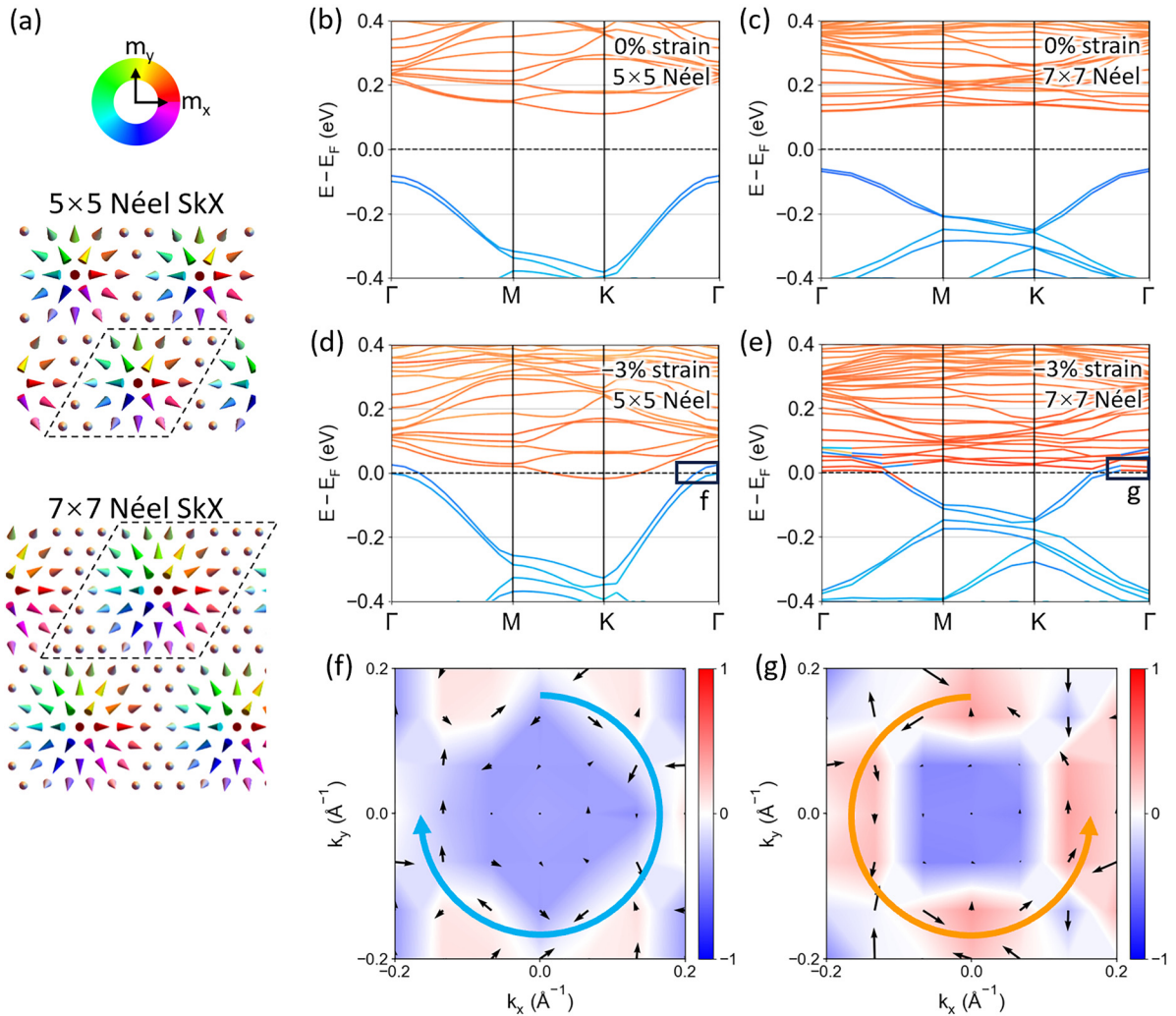


FIG. 4. Spin textures and band structures of skyrmion crystal (SkX) in LiCrTe_2 supercell. (a) Spin textures in SkX with skyrmions of 5×5 (upper panel) and 7×7 (lower panel) supercell size. Each arrow indicates a localized magnetic moment of a Cr atom in real space. The dashed boxes represent the corresponding periodic supercells. (b) and (c) Band structures of Néel-type SkX in LiCrTe_2 with skyrmions of 5×5 and 7×7 supercell size without strain. The orange and blue colors of bands represent the conduction and valence bands that are mainly contributed by Cr and Te atoms, respectively. (d) and (e) Band structures of supercells with -3% biaxial strain applied to single-layer LiCrTe_2 . (f) Spin textures in reciprocal space of the valence band maximum of 5×5 supercells SkX in LiCrTe_2 under -3% biaxial strain. The k -mesh is set in the X - Y plane around the Γ point. (g) Spin textures of the conduction band minimum when the supercell of SkX increases to 7×7 under -3% biaxial strain, where the valence bands cross with conducting bands and change the spin textures chirality.

inverse relationship between the electronic band gap and the skyrmion size in the SkX.

The supercells in the SkX exhibit consistent chirality of spin textures in both real and reciprocal space. This consistency, however, is disrupted when the conduction bands intersect with valence bands, which leads to a reversal of chirality in spin textures of reciprocal space while the skyrmions still maintain Néel type. A notable effect of compressive strain on the skyrmion lattice is inducing the band gap. As shown in Fig. 4(d), upon applying a -3% biaxial strain to the unit cell of single-layer LiCrTe_2 where the lattice constant becomes 4.0 \AA , the indirect gap in the 5×5 supercell decreases. More intriguingly, when the skyrmion size increases to a 7×7 supercell, a band crossing occurs, as shown in Fig. 4(e). Given that the valence band maximum (VBM) and conduction band minimum are contributed by

Te and Cr atoms, respectively, the band inversion leads to a notable variation of spin textures in the momentum space of the SkX. Figures 4(f) and 4(g) illustrate this phenomenon by demonstrating the transition of the VBM of the SkX in the strained LiCrTe_2 , which performs a reversal from left to right chirality of spin textures in reciprocal space as the skyrmion size increases from 5×5 to 7×7 supercells. Consequently, since the size of skyrmions is associated with the density of the SkX, we can conclude that the electronic properties in reciprocal space are influenced by the topological properties of the magnetic structure in real space. In a SkX comprising skyrmions of 5×5 supercell size, the diameter of the skyrmions measures 2.1 nm , whereas in a 7×7 supercell size, the diameter increases to 2.9 nm . The size of skyrmions is significantly influenced by variations in spin textures due to different magnetic field strengths. As a result, the associated

electronic band properties can be further adjusted through external fields and strain, providing multiple avenues for tuning the bands. These also suggest the potential to combine the anomalous Hall effect with the topological Hall effect in magnetic materials that possess topological bands.

IV. CONCLUSIONS

In conclusion, we investigated the complex spin textures in monolayer LiCrTe_2 and analyzed the evolution of a Néel-type SkX under varying temperatures and magnetic fields through first-principles-derived micromagnetic simulations. The high stability of magnetic properties of LiCrTe_2 enables the monolayer to sustain skyrmions at temperatures up to ~ 150 K, with a SkX emerging under magnetic fields ranging from 4 to 9 T. First-principles calculations have also confirmed the presence of a Néel-type SkX in single-layer LiCrTe_2 and observed that the band gap of the SkX decreases as the size of the skyrmions increases. Band gap closing and crossing occurred when the skyrmion size changed from a 5×5 to a 7×7 supercell under -3% biaxial strain on the LiCrTe_2 lattice,

leading to a reversal in both the electronic band structure and the chirality of spin textures in momentum space. In this paper, we prove the LiCrTe_2 monolayer as a high-density SkX and provide insights into the emergence of topological charge related to spin textures in 2D magnetic materials. The correlation between electronic bands and spin textures also gives the potential for integrating the tunable anomalous Hall effect with the topological Hall effect, offering promising prospects for future spintronic applications.

ACKNOWLEDGMENTS

We acknowledge financial support from the National Key Research and Development Program of China (Grants No. 2020YFA0308800 and No. 2021YFA1400201), National Natural Science Foundation of China (Grants No. 12025407, No. 12450401, No. 12374172, and No. 12321004), and Chinese Academy of Sciences (Grants No. YSBR047 and No. XDB330301). The computational resources in our studies we used were provided by the Shanghai Supercomputing Center, Institute of Physics Chinese Academy of Sciences and Songshan Lake Materials Laboratory.

-
- [1] S. Kumari, D. K. Pradhan, N. R. Pradhan, and P. D. Rack, Recent developments on 2D magnetic materials: Challenges and opportunities, *Emergent Mater.* **4**, 827 (2021).
- [2] Z. Liao, P. Jiang, Z. Zhong, and R.-W. Li, Materials with strong spin-textured bands, *npj Quantum Mater.* **5**, 30 (2020).
- [3] Y. Shoji and T. Mizumoto, Magneto-optical non-reciprocal devices in silicon photonics, *Sci. Technol. Adv. Mater.* **15**, 014602 (2014).
- [4] S.-h. Noh, S. H. Moon, T.-H. Shin, Y. Lim, and J. Cheon, Recent advances of magneto-thermal capabilities of nanoparticles: From design principles to biomedical applications, *Nano Today* **13**, 61 (2017).
- [5] H. H. Kim, B. Yang, S. Tian, C. Li, G.-X. Miao, H. Lei, and A. W. Tsen, Tailored tunnel magnetoresistance response in three ultrathin chromium trihalides, *Nano Lett.* **19**, 5739 (2019).
- [6] A. Matsui, T. Nomoto, and R. Arita, Skyrmion-size dependence of the topological Hall effect: A real-space calculation, *Phys. Rev. B* **104**, 174432 (2021).
- [7] H. Wang, Y. Dai, G.-M. Chow, and J. Chen, Topological Hall transport: Materials, mechanisms and potential applications, *Prog. Mater. Sci.* **130**, 100971 (2022).
- [8] S. Chen, S. Yuan, Z. Hou, Y. Tang, J. Zhang, T. Wang, K. Li, W. Zhao, X. Liu, L. Chen *et al.*, Recent progress on topological structures in ferroic thin films and heterostructures, *Adv. Mater.* **33**, 2000857 (2021).
- [9] G. Yu, P. Upadhyaya, Q. Shao, H. Wu, G. Yin, X. Li, C. He, W. Jiang, X. Han, P. K. Amiri *et al.*, Room-temperature skyrmion shift device for memory application, *Nano Lett.* **17**, 261 (2017).
- [10] X. Yu, N. Kanazawa, W. Zhang, T. Nagai, T. Hara, K. Kimoto, Y. Matsui, Y. Onose, and Y. Tokura, Skyrmion flow near room temperature in an ultralow current density, *Nat. Commun.* **3**, 988 (2012).
- [11] Y. Tokunaga, X. Yu, J. White, H. M. Rønnow, D. Morikawa, Y. Taguchi, and Y. Tokura, A new class of chiral materials hosting magnetic skyrmions beyond room temperature, *Nat. Commun.* **6**, 7638 (2015).
- [12] Q. Qin, L. Liu, W. Lin, X. Shu, Q. Xie, Z. Lim, C. Li, S. He, G. M. Chow, and J. Chen, Emergence of topological Hall effect in a SrRuO_3 single layer, *Adv. Mater.* **31**, 1807008 (2019).
- [13] Y. Li, S. Xu, J. Wang, C. Wang, B. Yang, H. Lin, W. Duan, and B. Huang, Interplay between quantum anomalous Hall effect and magnetic skyrmions, *Proc. Natl. Acad. Sci. USA* **119**, e2122952119 (2022).
- [14] D.-L. Bao, A. O'Hara, S. Du, and S. T. Pantelides, Tunable, ferroelectricity-inducing, spin-spiral magnetic ordering in monolayer FeOCl , *Nano Lett.* **22**, 3598 (2022).
- [15] Y. Wu, S. Zhang, J. Zhang, W. Wang, Y. L. Zhu, J. Hu, G. Yin, K. Wong, C. Fang, C. Wan *et al.*, Néel-type skyrmion in $\text{WTe}_2/\text{Fe}_3\text{GeTe}_2$ van der Waals heterostructure, *Nat. Commun.* **11**, 3860 (2020).
- [16] S. Jaiswal, K. Litzius, I. Lemesch, F. Büttner, S. Finizio, J. Raabe, M. Weigand, K. Lee, J. Langer, B. Ocker *et al.*, Investigation of the Dzyaloshinskii-Moriya interaction and room temperature skyrmions in W/CoFeB/MgO thin films and microwires, *Appl. Phys. Lett.* **111**, 022409 (2017).
- [17] X. Wang, H. Yuan, and X. Wang, A theory on skyrmion size, *Commun. Phys.* **1**, 31 (2018).
- [18] H. Wu, X. Hu, K. Jing, and X. Wang, Size and profile of skyrmions in skyrmion crystals, *Commun. Phys.* **4**, 210 (2021).
- [19] P. Li, J. Ding, S. S.-L. Zhang, J. Kally, T. Pillsbury, O. G. Heinonen, G. Rimal, C. Bi, A. DeMann, S. B. Field *et al.*, Topological Hall effect in a topological insulator interfaced with a magnetic insulator, *Nano Lett.* **21**, 84 (2020).
- [20] X. Li *et al.*, Topological Kerr effects in two-dimensional magnets with broken inversion symmetry, *Nat. Phys.* **20**, 1145 (2024).
- [21] X. Yu, D. Morikawa, T. Yokouchi, K. Shibata, N. Kanazawa, F. Kagawa, T.-h. Arima, and Y. Tokura, Aggregation and collapse dynamics of skyrmions in a non-equilibrium state, *Nat. Phys.* **14**, 832 (2018).
- [22] T. Kurumaji, T. Nakajima, M. Hirschberger, A. Kikkawa, Y. Yamasaki, H. Sagayama, H. Nakao, Y. Taguchi, T.-h. Arima,

- and Y. Tokura, Skyrmion lattice with a giant topological Hall effect in a frustrated triangular-lattice magnet, *Science* **365**, 914 (2019).
- [23] J.-J. Xian, C. Wang, J.-H. Nie, R. Li, M. Han, J. Lin, W.-H. Zhang, Z.-Y. Liu, Z.-M. Zhang, M.-P. Miao *et al.*, Spin mapping of intralayer antiferromagnetism and field-induced spin reorientation in monolayer CrTe₂, *Nat. Commun.* **13**, 257 (2022).
- [24] W. Xu, S. Ali, Y. Jin, X. Wu, and H. Xu, Intrinsic ferromagnetic semiconductors in two-dimensional alkali-based chromium chalcogenides, *ACS Appl. Electron. Mater.* **2**, 3853 (2020).
- [25] Q. Cui, J. Liang, Z. Shao, P. Cui, and H. Yang, Strain-tunable ferromagnetism and chiral spin textures in two-dimensional Janus chromium dichalcogenides, *Phys. Rev. B* **102**, 094425 (2020).
- [26] W. Du, K. Dou, Z. He, Y. Dai, B. Huang, and Y. Ma, Spontaneous magnetic skyrmions in single-layer CrInX₃ (X = Te, Se), *Nano Lett.* **22**, 3440 (2022).
- [27] P. Li, Q. Cui, Y. Ga, J. Liang, and H. Yang, Large Dzyaloshinskii-Moriya interaction and field-free topological chiral spin states in two-dimensional alkali-based chromium chalcogenides, *Phys. Rev. B* **106**, 024419 (2022).
- [28] J. Huang, B. Shi, F. Pan, J. Wang, J. Liu, D. Xu, H. Zhang, T. Xia, and P. Cheng, Anisotropic magnetic properties and tunable conductivity in two-dimensional layered NaCrX₂ (X = Te, Se, S) single crystals, *Phys. Rev. Mater.* **6**, 094013 (2022).
- [29] E. Nocerino, C. Witteveen, S. Kobayashi, O. K. Forslund, N. Matsubara, A. Zubayer, F. Mazza, S. Kawaguchi, A. Hoshikawa, I. Umegaki *et al.*, Nuclear and magnetic spin structure of the antiferromagnetic triangular lattice compound LiCrTe₂ investigated by μ^+ SR, neutron and x-ray diffraction, *Sci. Rep.* **12**, 21657 (2022).
- [30] C. Witteveen, E. Nocerino, S. A. López-Paz, H. O. Jeschke, V. Y. Pomjakushin, M. Månsson, and F. O. von Rohr, Synthesis and anisotropic magnetic properties of LiCrTe₂ single crystals with a triangular-lattice antiferromagnetic structure, *J. Phys. Mater.* **6**, 035001 (2023).
- [31] J. Liu, B. Ding, J. Liang, X. Li, Y. Yao, and W. Wang, Magnetic Skyrmionic bubbles at room temperature and sign reversal of the topological Hall effect in a layered ferromagnet Cr_{0.87}Te, *ACS Nano* **16**, 13911 (2022).
- [32] C. Zhang, C. Liu, J. Zhang, Y. Yuan, Y. Wen, Y. Li, D. Zheng, Q. Zhang, Z. Hou, G. Yin *et al.*, Room-temperature magnetic skyrmions and large topological Hall effect in chromium telluride engineered by self-intercalation, *Adv. Mater.* **35**, 2205967 (2023).
- [33] P. Jiang, L. Li, Z. Liao, Y. Zhao, and Z. Zhong, Spin direction-controlled electronic band structure in two-dimensional ferromagnetic CrI₃, *Nano Lett.* **18**, 3844 (2018).
- [34] G. Kresse and D. Joubert, From ultrasoft pseudopotentials to the projector augmented-wave method, *Phys. Rev. B* **59**, 1758 (1999).
- [35] J. P. Perdew, K. Burke, and M. Ernzerhof, Generalized gradient approximation made simple, *Phys. Rev. Lett.* **77**, 3865 (1996).
- [36] P. E. Blöchl, Projector augmented-wave method, *Phys. Rev. B* **50**, 17953 (1994).
- [37] A. Togo, First-principles phonon calculations with PHONOPY and PHONO3PY, *J. Phys. Soc. Jpn.* **92**, 012001 (2023).
- [38] A. Vansteenkiste, J. Leliaert, M. Dvornik, M. Helsen, F. Garcia-Sanchez, and B. Van Waeyenberge, The design and verification of MUMAX3, *AIP Advances* **4**, 107133 (2014).
- [39] See Supplemental Material at <http://link.aps.org/supplemental/10.1103/PhysRevB.111.054423> for phonon bands and more electronic band structures, four-state method calculation, and more details about spin textures width, which includes Refs. [40,46].
- [40] H. J. Xiang, E. J. Kan, S.-H. Wei, M.-H. Whangbo, and X. G. Gong, Predicting the spin-lattice order of frustrated systems from first principles, *Phys. Rev. B* **84**, 224429 (2011).
- [41] H. Xiang, C. Lee, H.-J. Koo, X. Gong, and M.-H. Whangbo, Magnetic properties and energy-mapping analysis, *Dalton Trans.* **42**, 823 (2013).
- [42] W. Pan, C. Xu, X. Li, Z. Xu, B. Liu, B.-L. Gu, and W. Duan, Chiral magnetism in lithium-decorated monolayer CrTe₂: Interplay between Dzyaloshinskii-Moriya interaction and higher-order interactions, *Phys. Rev. B* **109**, 214405 (2024).
- [43] X.-C. Hu, H.-T. Wu, and X. Wang, A theory of skyrmion crystal formation, *Nanoscale* **14**, 7516 (2022).
- [44] C. Xu, J. Feng, S. Prokhorenko, Y. Nahas, H. Xiang, and L. Bellaiche, Topological spin texture in Janus monolayers of the chromium trihalides Cr(I, X)₃, *Phys. Rev. B* **101**, 060404(R) (2020).
- [45] Y. Tokura and N. Kanazawa, Magnetic skyrmion materials, *Chem. Rev.* **121**, 2857 (2020).
- [46] I. S. Lobanov, H. Jónsson, and V. M. Uzdin, Mechanism and activation energy of magnetic skyrmion annihilation obtained from minimum energy path calculations, *Phys. Rev. B* **94**, 174418 (2016).